# Thirteen-velocity three-dimensional lattice Boltzmann model

Dominique d'Humières[1,2,*] M'hamed Bouzidi,[1,†] and Pierre Lallemand[1,‡]
[1]Laboratoire CNRS-ASCI, Bâtiment 506, Université Paris-Sud (Paris XI Orsay), 91405 Orsay Cedex, France
[2]Laboratoire de Physique Statistique, ENS, 24 Rue Lhomond 75231 Paris Cédex 05, France
(Received 30 November 2000; published 21 May 2001)

A thirteen-velocity three-dimensional lattice Boltzmann model on a cubic grid is presented. The transport coefficients derived from the standard Chapman-Enskog expansion are given together with the conditions for isotropy and Galilean invariance. The different invariants of the model are discussed. The results of measurements of drag and torque on a free falling sphere in a cylinder are in good agreement with solutions of the Navier-Stokes equation. Comparison of the time evolution of a freely decaying Taylor-Green vortex computed by fast Fourier transform and by the present model is presented.

DOI: 10.1103/PhysRevE.63.066702 PACS number(s): 02.70.Ns, 47.10.+g, 47.11.+j, 05.20.Dd

## I. INTRODUCTION

Lattice Boltzmann fluids (LBF) have been considered for the last ten years or so as possible fictitious media useful to perform small Mach number direct Navier Stokes simulations. The basic principle consists in computing the time evolution of the distribution function of fictitious particles that move synchronously along the links of a lattice of high symmetry. We recall that a LBF model is defined by several ingredients: a set of nodes where the particles are located, a set of rules for their motion (often going from one node to its close neighbors) to represent molecular advection using a small set of possible molecular velocities (here 13 of them) and a set of rules for the redistribution of particles present on each node to mimic collision processes in a real fluid.

Many systems have been used for both two and three dimensional cases. Originating from the simpler lattice gas models (LGA) introduced by [1], lattice Boltzmann fluids are usually based on a simple grid: square or hexagonal in two-dimensions (2D) and simple cubic in 3D. This allows us to use very simple algorithms to perform the simulations.

Here we shall consider a three-dimensional model on a cubic grid including collisions that follow a multirelaxation process [2] that possesses many more degrees of freedom than the commonly used Bhatnagar-Gross-Krook (BGK) models [3,4]. The model presented in Sec. II uses thirteen velocities, probably the minimal set of velocities in three dimensions allowing us to get the correct Navier-Stokes equation in terms of Galilean invariance and isotropy. This model has several invariants that will be presented and discussed in Sec. III. It turns out to be quite efficient to perform moderate Reynolds flow simulations and we shall give some results obtained for a sphere falling in a cylinder in Sec. IV A and for the free decay of a Taylor-Green vortex in Sec. IV B. In both cases we shall compare the data obtained with the LBF model with those coming from standard techniques in (CFD) [Galerkin or fast Fourier transform (FFT)].

## II. DEFINITION OF THE MODEL

The LBF model considered is defined on a cubic grid with unit length 1 (all quantities will be given in nondimensional units). During the displacement step of the LBF cycle, the populations move from one node of the grid to itself or to one of its second neighbors. Taking $\delta t=1$ for the duration of the unit time step, this leads to the set of possible velocities:

$$\begin{aligned}
&\vec{c}_0=(0,0,0),\\
&\vec{c}_1=(1,1,0),\quad \vec{c}_7=(-1,-1,0),\\
&\vec{c}_2=(1,-1,0),\quad \vec{c}_8=(-1,1,0),\\
&\vec{c}_3=(1,0,1),\quad \vec{c}_9=(-1,0,-1),\\
&\vec{c}_4=(1,0,-1),\quad \vec{c}_{10}=(-1,0,1),\\
&\vec{c}_5=(0,1,1),\quad \vec{c}_{11}=(0,-1,-1),\\
&\vec{c}_6=(0,1,-1),\quad \vec{c}_{12}=(0,-1,1).
\end{aligned} \tag{1}$$

On each node of the computational domain, the LBF is then characterized by thirteen populations corresponding to these thirteen velocities,

$$\mathbf{N}(\vec{r},t)\equiv(N_0(\vec{r},t),N_1(\vec{r},t),\ldots,N_{12}(\vec{r},t)). \tag{2}$$

Note that we distinguish vectors in real space $\mathbb{R}^3$ such as $\vec{r}$, with components $x$, $y$, and $z$ labeled by greek indices, and vectors in velocity space $\mathbb{R}^{13}$ such as $\mathbf{N}$, with components 0 to 12 labeled by latin indices.

The time evolution of the state of the fluid follows the general equation

$$N_i(\vec{r}+\vec{c}_i,t+1)=N_i(\vec{r},t)-\sum_{j=0}^{12} C_{ij}[N_j(\vec{r},t)-N_j^{\mathrm{eq}}(\vec{r},t)], \tag{3}$$

where $\mathbf{N}^{\mathrm{eq}}$ is the equilibrium distribution and $\mathcal{C}=\{C_{ij}\}$ is the collision operator, both being defined below using the "moment analysis" introduced in [2].

*Electronic address: dominique.dhumieres@lps.ens.fr
†Electronic address: bouzidi@asci.fr
‡Electronic address: lalleman@asci.fr

 

For this purpose we first define thirteen pairwise orthogonal vectors $\mathbf{e}_k$, $k\in\{0,\ldots,12\}$, in the 13-velocity space spanned by the $\vec{c}_i$:

$$\begin{aligned}
\mathbf{e}_0&=(1,1,1,1,1,1,1,1,1,1,1,1,1)=(c_i^0),\\
\mathbf{e}_1&=(0,1,1,1,1,0,0,-1,-1,-1,-1,0,0)=(c_{ix}),\\
\mathbf{e}_2&=(0,1,-1,0,0,1,1,-1,1,0,0,-1,-1)=(c_{iy}),\\
\mathbf{e}_3&=(0,0,0,1,-1,1,-1,0,0,-1,1,-1,1)=(c_{iz}),\\
\mathbf{e}_4&=(-12,1,1,1,1,1,1,1,1,1,1,1,1)=(13c_i^2/2-12c_i^0),\\
\mathbf{e}_5&=(0,1,1,1,1,-2,-2,1,1,1,1,-2,-2)=(3c_{ix}^2-c_i^2),\\
\mathbf{e}_6&=(0,1,1,-1,-1,0,0,1,1,-1,-1,0,0)=(c_{iy}^2-c_{iz}^2),\\
\mathbf{e}_7&=(0,1,-1,0,0,0,0,1,-1,0,0,0,0)=(c_{ix}c_{iy}),\\
\mathbf{e}_8&=(0,0,0,0,0,1,-1,0,0,0,0,1,-1)=(c_{iy}c_{iz}),\\
\mathbf{e}_9&=(0,0,0,1,-1,0,0,0,0,1,-1,0,0)=(c_{ix}c_{iz}),\\
\mathbf{e}_{10}&=(0,1,1,-1,-1,0,0,-1,-1,1,1,0,0)=(c_{ix}(c_{iy}^2-c_{iz}^2)),\\
\mathbf{e}_{11}&=(0,-1,1,0,0,1,1,1,-1,0,0,-1,-1)=(c_{iy}(c_{iz}^2-c_{ix}^2)),\\
\mathbf{e}_{12}&=(0,0,0,1,-1,-1,1,0,0,-1,1,1,-1)=(c_{iz}(c_{ix}^2-c_{iy}^2)),
\end{aligned}\tag{4}$$

with $c_0=||\vec{c}_0||=0$ and $c_i=||\vec{c}_i||=\sqrt{2}$ for $i\in\{1,\ldots,12\}$.

Then the population vector $\mathbf{N}$ is projected on the $\mathbf{e}_k$'s, defining 13 moments $M_k$

$$M_k=\mathbf{N}\cdot\mathbf{e}_k=\sum_{i=0}^{12}N_i e_{ki},\quad k\in\{0,\ldots,12\}. \tag{5}$$

At this point it is convenient to relate these moments to physical quantities

$$(M_0,M_1,\ldots,M_{12})\equiv(\rho,j_x,j_y,j_z,e,3S_{xx},S_{ww},S_{xy},S_{yz},S_{xz},h_x,h_y,h_z), \tag{6}$$

where the elements of the right-hand side correspond to the density, the mass fluxes along *x*, *y*, and *z*, a scalar related to the kinetic energy, five components related to the viscous stress tensor [note that $S_{yy}=(S_{ww}-S_{xx})/2$, $S_{zz}=-(S_{ww}+S_{xx})/2$, and $S_{xx}+S_{yy}+S_{zz}=0$], and the components of a 3D vector without obvious physical meaning.

The collision operator is now chosen such that the 13 moments $M_k$ are its eigenvectors with corresponding eigenvalues $\lambda_k$ (between 0 and 2 for linear stability). The first four moments are the conserved quantities and their associated eigenvalues are irrelevant for the dynamics [see Eq. (21) below]. In order to reflect the symmetries of the cubic lattice the nine other eigenvalues must be chosen such that

$$(\lambda_4,\lambda_5,\ldots,\lambda_{12})\equiv(\lambda_e,\lambda_\nu,\lambda_\nu,\lambda'_\nu,\lambda'_\nu,\lambda'_\nu,\lambda_h,\lambda_h,\lambda_h). \tag{7}$$

In order to recover the Navier-Stokes equation for an athermal fluid the values of the moments at equilibrium must be chosen as

$$M_0^{\rm eq}=\rho, \tag{8}$$

$$M_1^{\rm eq}=j_x, \tag{9}$$

$$M_2^{\rm eq}=j_y, \tag{10}$$

$$M_3^{\rm eq}=j_z, \tag{11}$$

$$M_4^{\rm eq}=e^{\rm eq}=\frac{3}{2}(13c_s^2-8)\rho+\frac{13}{2\rho}(j_x^2+j_y^2+j_z^2), \tag{12}$$

$$M_5^{\rm eq}=3S_{xx}^{\rm eq}=\frac{2j_x^2-(j_y^2+j_z^2)}{\rho}, \tag{13}$$

$$M_6^{\rm eq}=S_{ww}^{\rm eq}=\frac{j_y^2-j_z^2}{\rho}, \tag{14}$$

$$M_7^{\rm eq}=S_{xy}^{\rm eq}=\frac{j_xj_y}{\rho}, \tag{15}$$

$$M_8^{\rm eq}=S_{yz}^{\rm eq}=\frac{j_yj_z}{\rho}, \tag{16}$$

$$M_9^{\rm eq}=S_{xz}^{\rm eq}=\frac{j_xj_z}{\rho}, \tag{17}$$

$$M_{10}^{\rm eq}=h_x^{\rm eq}=0, \tag{18}$$

$$M_{11}^{\rm eq}=h_y^{\rm eq}=0, \tag{19}$$

$$M_{12}^{\rm eq}=h_z^{\rm eq}=0. \tag{20}$$

Note that the so-called "incompressible" LBF [5] can be implemented by replacing $\rho$ by a constant $\rho_0$ in the denominators of the right-hand sides of Eqs. (12) to (17) and that Stokes flow can be obtained by setting the nonlinear terms equal to zero in the same equations.

Finally the time evolution of the LBF is not computed using Eq. (3), but rather

$$\mathbf{N}(\vec{r}+\vec{c}_i,t+1)=\mathbf{N}(\vec{r},t)-\sum_{k=4}^{12}\lambda_k\frac{M_k(\vec{r},t)-M_k^{\rm eq}(\vec{r},t)}{||\mathbf{e}_k||^2}\mathbf{e}_k. \tag{21}$$

A naive count of the operations required to compute the moments from Eq. (5) and the inverse projection in Eq. (21) yields respectively 93 and 69 additions/substractions. This count can be reduced to no more than 35 and 41 by computing only once the common subexpressions in Eq. (5) and Eq. (21).

Using the standard Chapman-Enskog expansion, this model leads to the continuity and Navier-Stokes equations

$$\partial_t \rho + \vec{\nabla} \cdot \vec{j} = 0, \tag{22}$$

$$\partial_t j_\alpha + \partial_\beta \left( \frac{j_\alpha j_\beta}{\rho} \right) = -c_s^2 \partial_\alpha \rho + \nu \Delta j_\alpha + \left( \frac{\nu}{3} + \zeta \right) \partial_\alpha (\vec{\nabla} \cdot \vec{j}), \tag{23}$$

where $c_s$ is the speed of sound and $\nu$ and $\zeta$ are the shear and bulk kinematic viscosities given by,

$$\nu = \frac{1}{4} \left( \frac{1}{\lambda_\nu} - \frac{1}{2} \right) = \frac{1}{2} \left( \frac{1}{\lambda'_\nu} - \frac{1}{2} \right), \quad \text{and}$$
$$\zeta = \frac{2 - 3c_s^2}{3} \left( \frac{1}{\lambda_e} - \frac{1}{2} \right). \tag{24}$$

Note that $\lambda_\nu$ and $\lambda'_\nu$ are different and related through the shear viscosity $\nu$; thus this model cannot be part of the single time relaxation (also called BGK) models. Therefore one cannot write a simple evolution equation for the $N_i$ making no reference to moments as was done in Ref. [3].

## III. INVARIANTS

### A. Checkerboard invariant

Since $c_{ix} + c_{iy} + c_{iy} \in \{-2,0,2\}$ for all $i \in \{0,1, \ldots ,12\}$, $x+y+z$ and $x+y+z+c_{ix}+c_{iy}+c_{iy}$ have the same parity for all $i \in \{0,1, \ldots ,12\}$. As a consequence two nodes having sums $x+y+z$ of different parity cannot exchange information during the time evolution. It follows that the cubic lattice can be split into two totally independent sublattices made of the nodes with $x+y+z$ even for one and odd for the other.

This checkerboard invariant can be removed by some simple geometrical transformations leading to the structure of the fcc lattice. The first one is a $\pi/4$ rotation around the $z$ axis: this gives a square lattice with a $\sqrt{2}$ mesh size in each $x'y'$ plane, with a spacing of 1 unit length in the $z$ direction; in addition the square lattice in the $x'y'$ planes with $z$ odd are shifted by $(1/\sqrt{2},1/\sqrt{2},0)$ with respect to the square lattice in the planes with $z$ even.

The second geometrical transformation takes the direction $(1,1,1)$ as the new $z'$ axis, the plane $x+y+z=0$ being the new $x'y'$ plane. This $x'y'$ plane contains the velocities $\{\vec{c}_2, \vec{c}_4, \vec{c}_6, \vec{c}_8, \vec{c}_{10}, \vec{c}_{12}\}$ that are the base vectors of a triangular lattice: this gives a triangular lattice with a $\sqrt{2}$ mesh size in each $x'y'$ plane, with a spacing of $2/\sqrt{3}$ in the $z'$ direction; in addition the triangular lattice in the $x'y'$ planes with $z' \equiv 1 \pmod 3$ are shifted by $(1/\sqrt{2},1/\sqrt{6},0)$, those with $z' \equiv -1 \pmod 3$ by $(-1/\sqrt{2},-1/\sqrt{6},0)$ with respect to the triangular lattice in the planes with $z' \equiv 0 \pmod 3$.

These two geometrical transformations lead to skewed mappings between the lattice and the storage array in a computer, similar to the one found when using triangular lattice. It is probably much better to use these two independent sublattices to simulate either two independent systems or two halves of the volume through appropriate boundary conditions as it is mentioned at the end of the Sec. IV C.

### B. Staggered invariant

With appropriate boundary conditions (such as infinite domain or periodic box with an even number of nodes in each direction) it is not difficult to see that

$$\sum_{x+y \in \mathbb{Z}_e, z \in \mathbb{Z}_e} j_z(x,y,z,t+1) - \sum_{x+y \in \mathbb{Z}_o, z \in \mathbb{Z}_o} j_z(x,y,z,t+1)$$
$$= (-1)^t \left( \sum_{x+y \in \mathbb{Z}_e, z \in \mathbb{Z}_e} j_z(x,y,z,t) - \sum_{x+y \in \mathbb{Z}_o, z \in \mathbb{Z}_o} j_z(x,y,z,t) \right), \tag{25}$$

where $\mathbb{Z}_e$ and $\mathbb{Z}_o$ are the sets of even and odd integers. This is one of the staggered invariants already known in other LBF such as $D3Q15$ or $D3Q19$. There are three such invariants for each sublattice. For the sublattice $x+y+z \in \mathbb{Z}_e$ the one given by Eq. (25) and two others obtained by exchanging $x$ or $y$ with $z$. And for the sublattice $x+y+z \in \mathbb{Z}_o$ one obtained by exchanging $x+y \in \mathbb{Z}_e$ and $x+y \in \mathbb{Z}_o$ in Eq. (25) and two others by exchanging $x$ or $y$ with $z$ afterwards.

It can also be checked that for the sublattice such that $x+y+z$ is even

$$\sum_{(x+y+z)/2 \in \mathbb{Z}_e} j_\perp(x,y,z,t+1) - \sum_{(x+y+z)/2 \in \mathbb{Z}_o} j_\perp(x,y,z,t+1)$$
$$= (-1)^t \left( \sum_{(x+y+z)/2 \in \mathbb{Z}_e} j_\perp(x,y,z,t) - \sum_{(x+y+z)/2 \in \mathbb{Z}_o} j_\perp(x,y,z,t) \right), \tag{26}$$

where $j_\perp$ is the mass flux in the direction $(1,1,1)$, perpendicular to the plane $x+y+z=0$. There are four such invariants for this sublattice, the three others being obtained by replacing the direction $(1,1,1)$ by $(-1,1,1)$, $(1,-1,1)$, and $(1,1,-1)$. The four invariants for the other sublattice are obtained by replacing $(x+y+z)/2$ by $(x+y+z+1)/2$ in Eq. (26). These invariants do not exist in the $D3Q15$ or $D3Q19$ models.

## IV. SIMULATIONS

As for other LBF models, parameters of the model must be chosen in order to avoid "run away" situations. As explained in detail elsewhere [6] this can be done by solving numerically the dispersion equation for modes that are periodic in space. A fast procedure allows to scan the various parameters of the model. After considering a broad range of values for the various parameters of the model, we can state that satisfactory results in terms of linear stability are obtained for

$$c_s^2=\frac{1}{3},$$

$$\lambda_e=1.5,$$

$$\lambda_\nu=1.0\text{–}1.96,$$

$$\lambda_h=1.8,$$

$c_s^2=1/3$ has been chosen to increase the stability of the model when the problem under study includes a constant drift velocity $V$ superimposed to features of small amplitude. (Note that the linear dependence in $V$ of the attenuation of sound waves propagating in the direction of the mean flow is anisotropic and cannot be put to 0 as for other 3D LBF models.) The values of $\lambda_e$ and $\lambda_h$ have been set to constant values chosen to have numerical stability over a broad range of viscosity (from $2.55\times10^{-3}$ to 0.125) for velocities up to 0.1 (in lattice units) without further tuning. Indeed it is very possible that a finer tuning of $\lambda_e$ and $\lambda_h$ as functions of $\lambda_\nu$ may increase the stability range in terms of maximum velocities or available Reynolds numbers. Such a study is beyond the scope of this paper and left as an exercise for the interested readers.

The usual relaxation of initial excitations periodic in space allows to verify that the transport coefficients given above are correct. In addition we verify that Galilean factors are equal to 1 when initial conditions include a uniform flow and a small periodic excitation.

### A. Stokes flow

We then consider a case that is discussed in the literature [8]. We compute a Stokes flow in a cylinder of radius $r_c$ and length $L_c$ in which a sphere of radius $r_s$ moves parallel to the axis of the cylinder at constant speed $-V$. The center of the sphere is located on the axis of the cylinder. We choose a frame of reference in which the sphere is fixed. Thus the walls of the cylinder move with velocity $V$. At the entrance and exit of the cylinder, we take a uniform profile with velocity $V$. The Stokes situation is achieved either by taking a low Reynolds number or more simply by putting the nonlinear terms in the equilibrium condition to zero.

To take into account the interaction of the fluid with the solid boundaries (sphere and cylinder) we use an extension of the bounce-back with linear interpolation for each link of the LBF lattice that connects a ''fluid'' and a ''solid'' point as described for the 2D case [7]. We then determine the momentum transfer between the fluid and the sphere at each time step. The component of the momentum transfer parallel to the axis of the cylinder is the drag of the sphere. When steady state is reached, we compare the measured drag to the Stokes value $6\pi\nu V r_s$. The ratio of these two quantities is larger than one for $r_s/r_c$ not very small. When the center of the sphere is no longer on the axis of the cylinder, but at a distance $d$, the flow produces a torque on the sphere proportional (for small $d/r_c$) to $8\pi\nu V r_s^2 d/r_c$ that can also be measured in the LBF simulations. This torque can be compared to the values computed by solving the Navier-Stokes equations with development of the velocity field on suitable functions. Table I gives the drag and the torque (times $r_c/d$) on the sphere in the units chosen by [8] (respectively, $6\pi\nu V r_s$ and $8\pi\nu V r_s^2$). The velocity and the geometry of the cylinder are given in the caption of Fig. 1. The simulations in this section and the next one have been performed with the ''incompressible'' version introduced in Sec. II with $\rho_0=1$.

TABLE I. Drag and torque in the sphere. The figures are given relative to the Stokes value ($6\pi\nu V r_s$) for the Drag and relative to $8\pi\nu V r_s^2$ for the torque times ($r_c/d$).

| | Drag | | (Torque)$\times(r_c/d)$ | |
|---|---|---|---|---|
| $r_s/r_c$ | LBF | Tözeren [8] | LBF | Tözeren [8] |
| 0.2 | 1.686 | 1.680 | | |
| 0.3 | 2.366 | 2.371 | 0.242 | 0.2466 |
| 0.4 | 3.574 | 3.593 | 0.604 | 0.6137 |
| 0.5 | 5.886 | 5.952 | 1.424 | 1.443 |
| 0.6 | 11.07 | 11.09 | 3.440 | 3.500 |

It is not possible to give a precise estimation of the relative accuracy of the determination of the momentum transfer

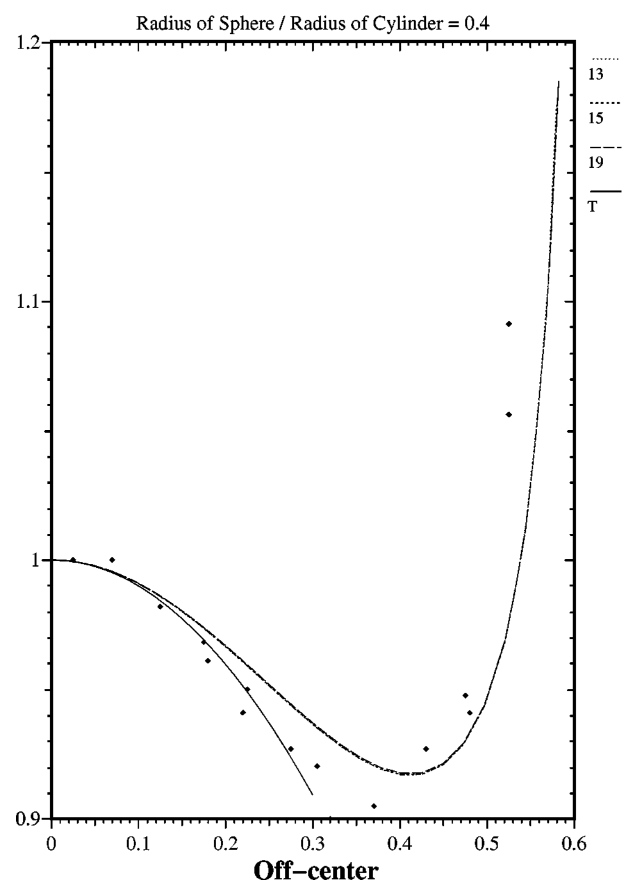


FIG. 1. Ratio $R$ between the drag determined for $d$ and its value for $d=0$ as a function of $d/r_c$, for $V=0.12$, $r_c=42.25$ and $L_c=459$ (in lattice units). The dotted, dashed, and long dashed curves correspond, respectively, to 13-, 15-, and 19-velocity models. The solid line is the polynomial expansion given by Tözeren [8]. The solid diamonds are the experimental points obtained by Ambari *et al.* [9] for $r_s/r_c=0.44$.

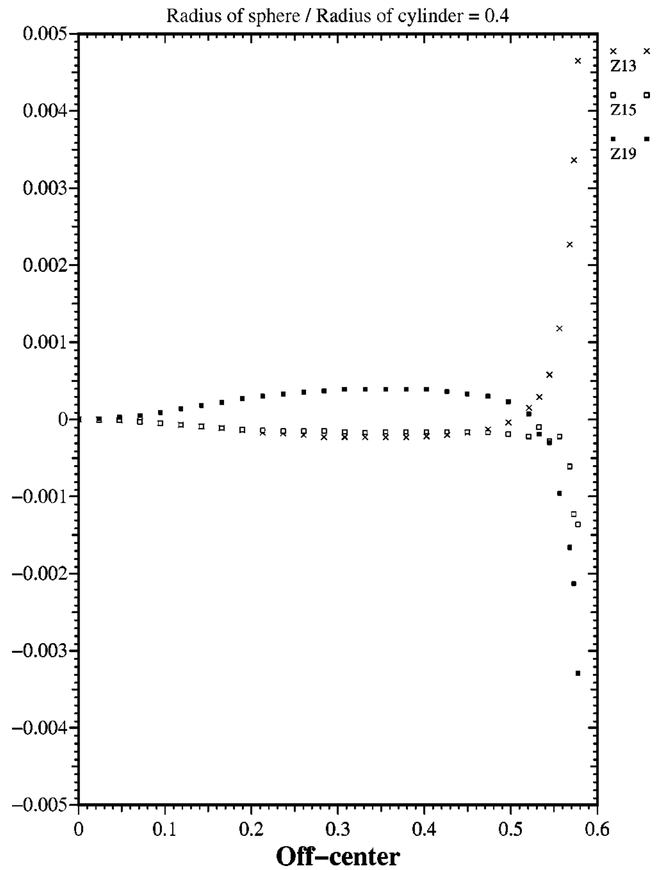


FIG. 2. Difference between the relative drags obtained for the three models and their average value as a function of $d/r_c$ for the same parameters as in Fig. 1.

measurement. The measured value of the torque is more sensitive to the detailed boundary conditions on the sphere especially when $r_s/r_c$ is small. The three-dimensional nature of the simulations prevented us from making an analysis similar to what is performed in Ref. [7] and to make precise statements concerning the observed dependency of the results with mesh size. We may add that a simpler description of the fluid-solid interaction in terms of ''bounce-back'' may also be used but leads to results that are more sensitive to the diameter of the sphere.

We then compare the predictions of LBF simulations for three models: the present 13-velocity model (referred to ''13''), the 15-velocity model using velocities {1,0,0} and {1,1,1} (referred to ''15'') and the 19 velocities using velocities {1,1,0} and {1,0,0} (referred to ''19''), see Ref. [3] for definitions of these models. Fluid-solid interaction are of the same type as for the 13-velocity model. We consider the same problem as above but we offset the center of the sphere with respect to the axis of the cylinder by a distance $d$ (expressed in units of $r_c$). For a fixed ratio $r_s/r_c=0.4$, we plot in Fig. 1 the ratio $R$ of the drag determined for $d$ to its value for $d=0$. For small $d$ the decrease of $R$ is in satisfactory agreement with the polynomial expansion given by Tözeren. At large value of $d$ we can only refer to experimental data [9] and we only claim qualitative agreement.

Figure 2 shows for the three LBF models the difference between the corresponding ratios $R$ and their average value. One can see that the maximum difference is smaller than 1%, even when the gap between the sphere and the cylinder is less than two lattice units.

### B. Taylor-Green vortex

After the test of the quality of the LBF model in the Stokes regime, we consider now a situation that has been used as a standard problem for turbulence problems: the time evolution of a Taylor-Green vortex [10]. We consider here the simple case of free decay from the initial conditions given below.

$$v_x(x,y,z,0)=u\,\sin(k_0x)\cos(k_0y)\cos(k_0z), \qquad (27)$$

$$v_y(x,y,z,0)=-u\,\cos(k_0x)\sin(k_0y)\cos(k_0z), \qquad (28)$$

$$v_z(x,y,z,0)=0. \qquad (29)$$

We then compute the time evolution of the corresponding flow with periodic boundary conditions in a cube of size $n^3$ with $k_0=2\pi/n$.

For small amplitude $u$, the flow decays as

$$\mathbf{v}(\mathbf{r},t)=\mathbf{v}(\mathbf{r},0)\exp(-3k_0^2\nu t),$$

where $\nu$ is the viscosity. This is verified with good accuracy.

For large values of $u$, the nonlinear terms in the Navier-Stokes equations lead to the appearance of spatial harmonics of the initial flow. We have measured the time evolution of the intensity (square of the amplitude) of a number of such spatial harmonics, both in a LBF simulation and in a FFT simulation. We show results in Fig. 3, where the solid lines correspond to LBF results and the dashed lines to FFT. The simulations are made on a $162^3$ domain (a small one by today's standards but large enough for our purposes) at an effective Reynolds number (defined by $\mathrm{Re}=un/\nu$) approximately equal to 1260. One can see that there is good overall agreement with differences in the amplitudes at the latest times of the simulation. The time is scaled to the reversal time of the initial vortex, the amplitudes are in arbitrary scales (the various curves are not indexed in terms of the wave number to keep the figure readable). A detailed examination of the present results allows us to make the following remarks.

The initial conditions satisfy div $\mathbf{v}=0$ and thus are well adapted for an incompressible flow simulation by FFT. Now for the value of $u\simeq0.095$ used in the LBF simulation the choice of the initial condition for the pressure field is important, for instance a uniform initial pressure leads to generation of additional spatial harmonics not present in FFT. To avoid this difficulty, the initial conditions for LBF included an appropriate pressure field closer to the one obtained from

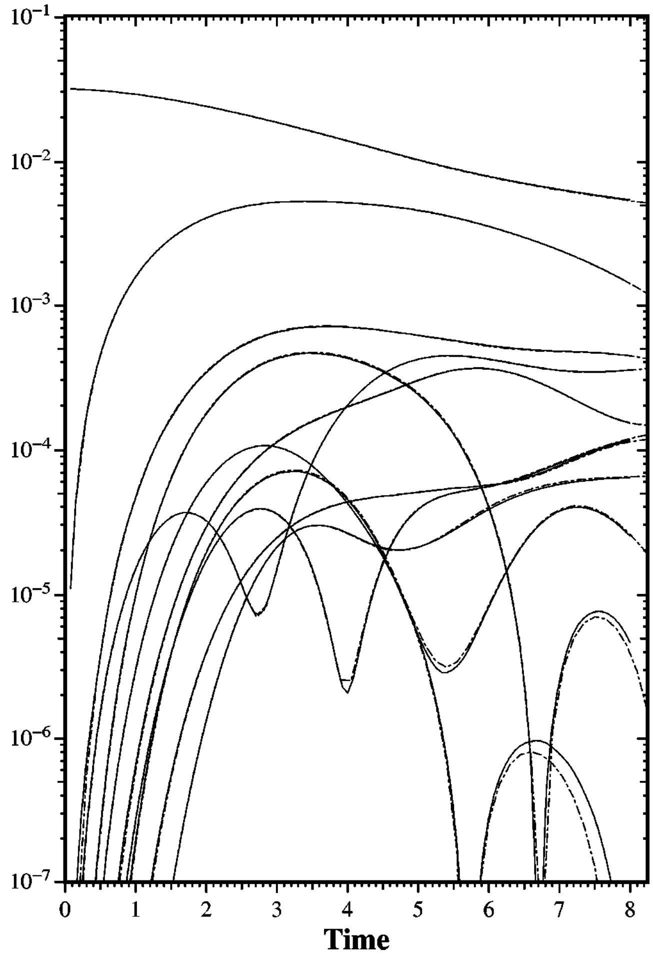


FIG. 3. Time evolution of the intensities (in arbitrary units) of some spatial harmonics of the Taylor-Green vortex, the solid lines correspond to LBF results and the dashed lines to FFT. The simulations are made on a $162^3$ domain at Re = 1260. Time is in units of reversal time of the initial vortex.

the time evolution of the flow. We then get a very good agreement between the time evolution of the total kinetic energy vs time computed by the two methods.

At the latest times shown in Fig. 3 one observes deviations in terms of intensity that may be attributed to two origins. As is well known in LBF (see Ref. [6] for a discussion) the macroscopic behavior at short spatial scales differs from that of a true Navier-Stokes fluid. This may be expressed in terms of $k$-dependent transport coefficients and value of the Galilean factor $g(\mathbf{k})$ that was introduced in the analysis of LGA. For the present LBF model we know how to compute $\nu(\mathbf{k})$ and how to include this information in the FFT code. When this is done there is only a minor improvement in the agreement between LBF and FFT. However, the way to properly introduce a $k$-dependent advection coefficient in a FFT code is less clear and has not been done. Note that the $k$ dependency of the viscosity in LBF can be seen as some kind of built-in ''hyperviscosity'' as those often used in FFT codes to avoid instabilities when using fairly large time steps.

For turbulence studies, using a ''noisy'' driving term in the FFT simulations is preferred. This can be done at very little cost in the LBF case, however this would make difficult separating various contributions to possible deviations between FFT and LBF.

We may add finally that on a given computer, producing the results of Fig. 3 takes comparable times using LBF or FFT (LBF is an order of magnitude faster per time step, but FFT allows to take larger time increments) and that LBF is much easier to parallelize and is far less costly in terms of data exchange between processors, a feature very useful when using clusters of low cost PC's. When we perform the same type of analysis with the 15 or 19 velocities LBF models we find very small differences in the LBF results. A detailed analysis of these findings would require a deep understanding of the influence of the $k$ dependence of $\nu$ and $g$ in a fully nonlinear problem.

### C. Invariants

Finally we have verified that the two sublattices $(i+j+k)$ even or odd are completely decoupled, allowing either to perform two independent simulations at the same time (this may be useful when studying the onset of instabilities as the two sublattices have different numerical ''noise'') or to optimize the use of computer memory (for instance in the situation discussed above, the even sublattice can be used to compute half the volume from the entrance and the odd sublattice for the remaining half to the exit with a suitable matching to connect them) or to optimize domain decomposition when making simulations on a parallel machine (we used a cluster of PC to perform the simulations discussed here).

## V. CONCLUSION

We have presented a simple and efficient LBF model for Navier-Stokes simulations. More work needs to be performed to find out the possible influence of the additional invariants discussed here. All our present simulations and analysis did not show any significant effect apart from the decoupling of the odd and even sublattices. Compared to the more commonly used 15 and 19 velocities LBF algorithms, the present model is very efficient as far as CPU time and memory requirements are concerned, but it has a somewhat higher shear viscosity for comparable numerical stability that should be considered when using LBF techniques for very large direct Navier-Stokes simulations.

## ACKNOWLEDGMENTS

The authors thank Dr. M. Meneguzzi for initiating them to FFT techniques and making his code available, and Professor A. Ambari for making his experimental data available.

[1] U. Frisch, B. Hasslacher, and Y. Pomeau, Phys. Rev. Lett. **56**, 1505 (1986).
[2] D. d'Humières, in *Rarefied Gas Dynamics: Theory and Simulations*, edited by B.D. Shizgal and D.P. Weaver, Progress in Astronautics and Aeronautics, Vol. 159 (AIAA, Washington, DC, 1992).
[3] Y.H. Qian, D. d'Humières, and P. Lallemand, Europhys. Lett. **17**, 479 (1992).
[4] H. Chen, S. Chen, and W.H. Matthaeus, Phys. Rev. A **45**, R5339 (1992).
[5] X. He and L.-S. Luo, J. Stat. Phys. **88**, 927 (1997).
[6] P. Lallemand and L.-S. Luo, Phys. Rev. E **61**, 6546 (2000).
[7] M. Bouzidi, M. Firdaous and P. Lallemand (unpublished).
[8] M. Tözeren, J. Fluid Mech. **129**, 77 (1983).
[9] A. Ambari, B. Gauthier-Manuel, and E. Guyon, J. Fluid Mech. **149**, 235 (1984).
[10] M.E. Brachet, D.I. Meiron, S.A. Orszag, B.G. Nickel, R.H. Morf, and U. Frisch, J. Fluid Mech. **130**, 411 (1983).